Chapter III: Experimental

This chapter discusses the methodology to synthesize the nanoparticles using co-precipitation technique in section 3.1. In order to examine the physical and chemical properties, various characterizations are performed. All characterization techniques used in the present work are discussed in section 3.2.

3.1 Synthesis of nanoparticles by co-precipitation technique

In normal precipitation, insoluble compounds are precipitated while in co-precipitation, soluble compounds are precipitated. In coprecipitation method, the calcination temperatures are usually lower than other mixed oxide methods and the products are easily milled to finer particle sizes. Co-precipitation can produce wide particle size distribution with mean size ranging from submicron to nanometer. $CoCr_2O_4$ and Zn doped $CoCr_2O_4$ nanoparticles were synthesized by wet chemical co-precipitation technique.

$CoCr_2O_4$ powders were synthesized by co-precipitation technique using the stoichiometric amount of stock solution of cobalt nitrate and chromium nitrate. Cobalt nitrate ($Co(No_3)_2.6H_2O$) of 99% purity and chromium nitrate ($Cr(No_3)_3.9H_2O$) of 98% purity purchased from Himedia Laboratories, India were mixed together after assay correction and were subjected to stirring using a magnetic stirrer. The mixed solution was subjected to continuous stirring at room temperature for 2h. Diluted aqueous ammonia (1 M NaOH) solution was added to the mixed solution under continuous stirring till complete precipitation to take place. The precipitate was filtered using Whatman's filter paper, washed several times with distilled water followed by acetone. Finally, it was left

for drying in an oven at 120°C for 16 h. In order to study the size dependent properties, the powders were calcined at 500 and 900°C for 4 hours. Samples calcined at 500°C and 900°C are expected to have different size due to grain growth. Detailed scheme of synthesis of $CoCr_2O_4$ is shown in Fig. 3.1.1.

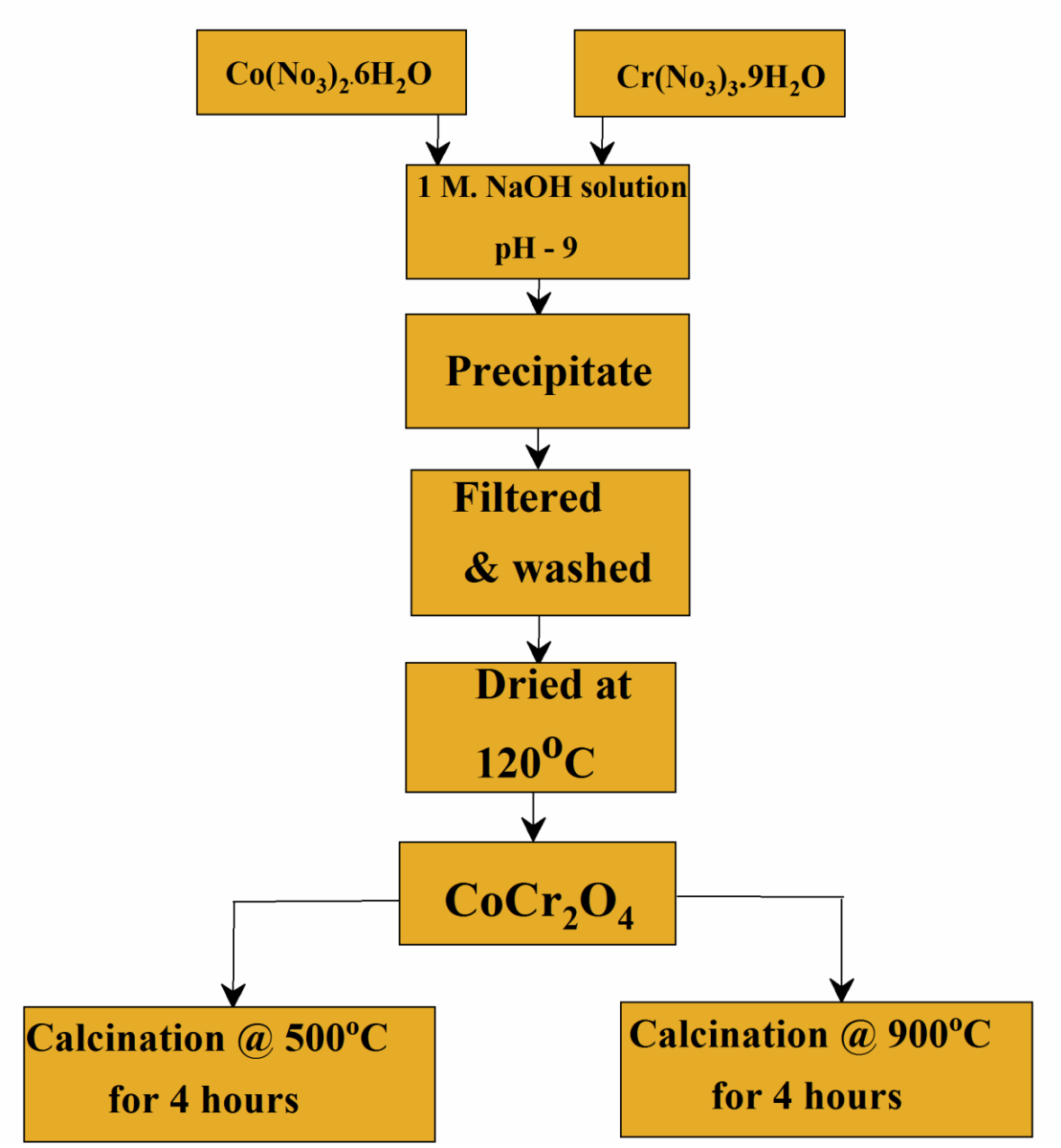

Fig. 3.1.1 Flow chart for synthesis of $CoCr_2O_4$ nanoparticles of different sizes.

Zn doped $CoCr_2O_4$ were also synthesized by chemical co-precipitation technique. Stoichiometric amounts of zinc nitrate ($Zn(No_3)_2.6H_2O$) with 99.5% purity, cobalt nitrate ($Co(No_3)_2.6H_2O$) of 99% purity and chromium nitrate ($Cr(No_3)_3.9H_2O$) of 98% purity were mixed together under continuous stirring. Diluted aqueous ammonia (1 M NaOH) solution was added to the mixed solution at room temperature till the pH value 9 was obtained. Precipitate was filtered using Whatman's filter paper and was washed several times with distilled water. Finally we washed with acetone. The sample was kept in oven at 120 ^oC for 16 h. As the powder is of amorphous in nature, we calcined the sample at 500^oC for 4 hours. Similarly, by taking appropriate amount of Zn nitrate in cobalt nitrate and chromium nitrate, we have prepared various Zn doped $CoCr_2O_4$ samples, i.e., $Zn_xCo_{1-x}Cr_2O_4$ (x=0.05, 0.1, 0.15, 0.2, 0.5, 0.8). For example, x=0.05 sample was prepared by taking 43.98 ml of $Co(No_3)_2.6H_2O$, 2.148 ml of ($Zn(No_3)_2.6H_2O$) and 44.358 ml of ($Cr(No_3)_3.9H_2O$) solutions. Finally the mechanical grinding was done to get a fine powder of particles for further measurements. The detailed flow chart of synthesis of $Zn_xCo_{1-x}Cr_2O_4$ is shown in Fig. 3.1.2.

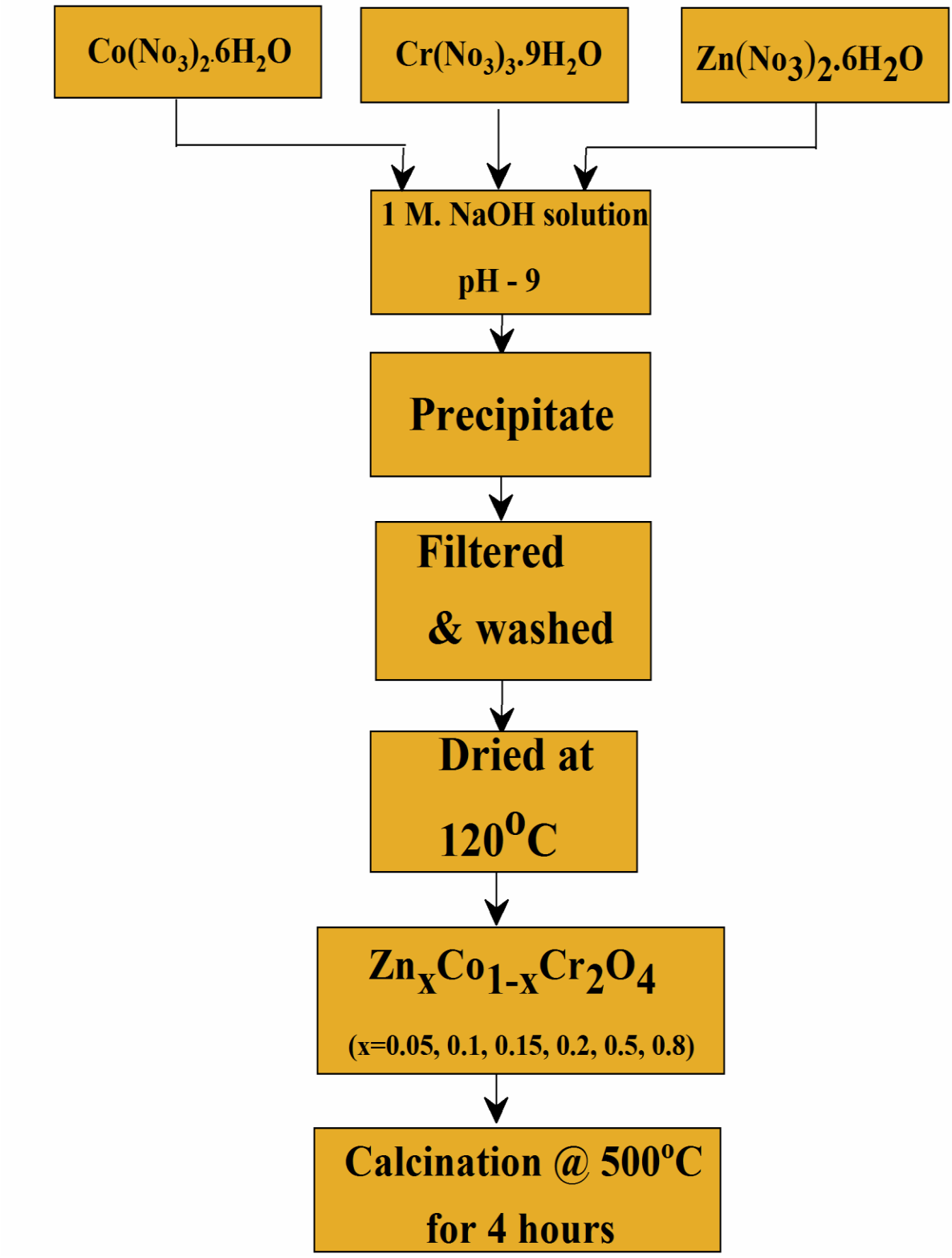

Fig.3.1.2 Experimental schematic diagram for synthesis of Zn doped $CoCr_2O_4$ nanoparticles.

3.2 Characterization techniques

$CoCr_2O_4$ and Zn doped $CoCr_2O_4$ samples calcined at 500^oC and 900^oC for 4 h were characterized using different techniques to understand their structure dependent physical properties. All the techniques used in the work are discussed below.

3.2.1 X-ray diffraction (XRD)

X-ray diffraction is one of the most powerful and non-destructive technique used to examine crystal structure of materials ranging from crystals to fluids. XRD technique is mainly used to identify the crystalline phase of the materials. XRD works on the principle of Bragg's law. According to Bragg's law, the diffracted X-rays from a set of equidistant parallel planes interfere constructively when the path difference between them is integral multiple of the incident wavelength of X-rays, i.e., $2d\sin\Theta=n\lambda$. Where, d is the inter-planar distance, Θ is Bragg angle, n is an integer known as order of the diffraction and λ is wavelength of incident X-rays [Cullity (1978)]. The schematic diagram of Bragg's law is shown in Fig. 3.2.1.

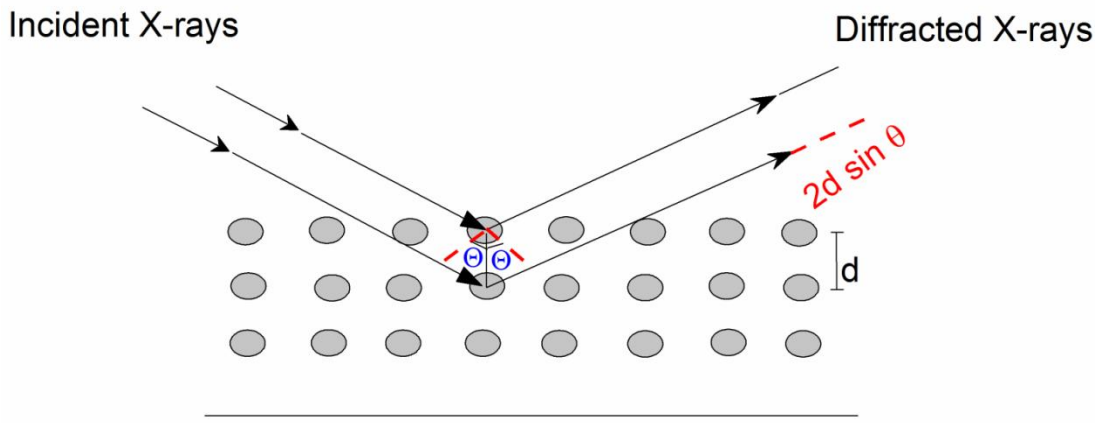

Fig.3.2.1 Schematic representation of incident and diffracted X-rays from the crystal lattice.

Very strong Bragg peaks are obtained in the diffraction pattern at the points where the scattering angles satisfy Bragg condition. In general, crystals with high symmetry tend to have relatively few atomic planes, whereas crystals with low symmetry (triclinic or monoclinic systems) possess large number of possible atomic planes in their structure. The possible direction of diffraction depends on the size and shape of the unit cell of the material. The kind and arrangement of atoms in the crystal structure affects the intensities of the diffracted waves.

XRD technique is mainly divided into 4 parts. 1. Production of X-rays, diffraction of X-rays from the material, detection of diffracted X-rays and interpretation of X-ray diffraction data. The schematic diagram of XRD is shown in Fig. 3.2.2.

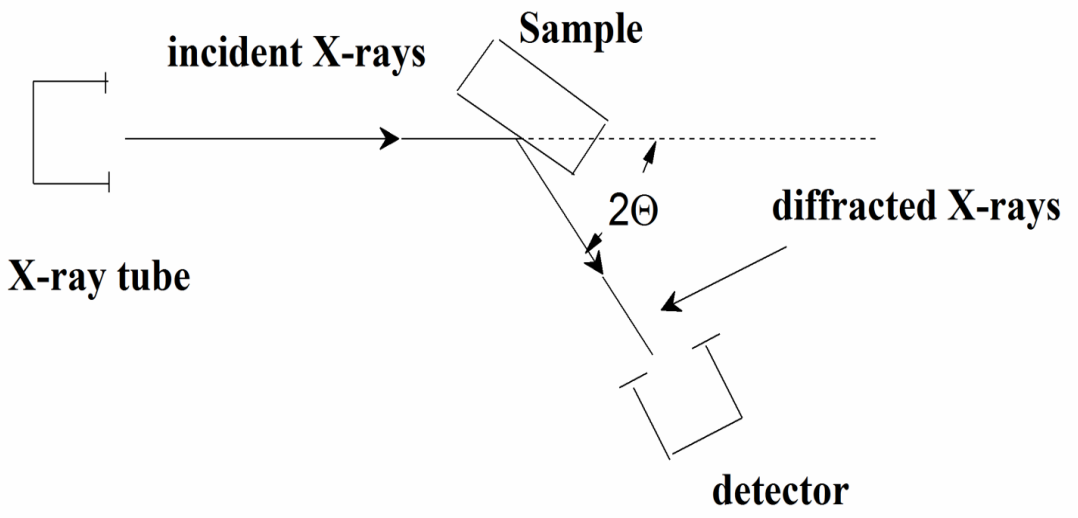

Fig. 3.2.2 Schematic representation of X-ray diffraction technique.

X-rays are produced when highly accelerated electrons collide with a Cu metal target. The characteristic X-rays (K_α) of wavelength 1.5418 Å are collimated and directed on to the material. The para-focusing (or Bragg-Brentano) diffractometer is the most

common geometry for diffraction instruments. The Bragg-Brentano geometry is best for samples having strong absorption. It requires flat sample surface and it could be easily adapted for in situ investigations. The diffracted X-rays from the test material are collected at the detector which converts the X-ray signals to a count rate. The sample rotates with an angle Θ, while the x-ray detector rotates with an angle of 2Θ. By measuring the angles and corresponding intensities of the diffracted beam, one can determine the crystal structure. For most of the powder samples, the typical value of 2Θ varies from 5^o to 120^o.

In present work, we used an 18 kW rotating anode (Cu K_α) based Rigaku (RINT 2000/PC series) powder diffractometer operating in the Bragg-Brentano geometry and fitted with a graphite monochromator in the diffracted beam which was used to record the diffraction patterns of the powder samples. The wavelength of the X-rays used was λ=1.5418 Å. The current and voltages was 100 mA and 40 kV with 2Θ ranging from 10-120^o. The XRD data was indexed and matched with Joint Committee on Powder Diffraction Standards data (JCPDS-780711) to confirm the pure phase of the prepared samples. Le-Bail analysis profile fitting technique was used to characterize the properties of crystalline materials. In this method, the suitable intensities were found to determine the atomic structure of a crystalline material and to refine the unit cell. The lattice parameter of unit cell was taken as 8.32 Å and Fd-3m space group was considered for the refinement. In order to perform well structural analysis and quantitative phase analysis, Hugo Rietveld devised a technique called as Rietveld refinement. This technique uses least squares approach to refine a theoretical line profile until it matches the observed profile. In general, it is a very useful technique when XRD data consists of overlapped

reflections, multiple phases and complex crystal structures. During refinement, pseudo-voigt function has been selected which have a combination of both Lorentzian and Gaussian distribution functions. The 6-coefficent polynomial function is considered as a background mode because the background data is found to be linear. The isotropic thermal parameter (B), occupancies are refined along with lattice parameter and atomic positions. The quality of the refinement is estimated from the χ^2 value which should be in between 0-1 for a good fit. The unit cell parameters, bond length, bond angle and various other structural parameters related to the crystal structure have been determined using Rietveld refinement. Both Le-Bail and Rietveld refinements are performed using Fullprof software package [Rodriguez-Carvajal (1990)].

3.2.2 X-ray Photoelectron Spectroscopy (XPS)

X-ray Photoelectron spectroscopy also known as Electron Spectroscopy for Chemical Analysis (ESCA) which is most widely used as surface analysis technique. It can be used for the quantitative analysis and to investigate the chemical state of the material. In XPS, the sample surface is excited with mono-energetic Al k_α X-rays which emit photoelectrons. The energy of the emitted photoelectrons is measured using electron energy analyzer. From the binding energy and intensity of a photoelectrons, the elements, its chemical state and quantity can be determined.

Principle: XPS is based on the principle of photoelectric effect. Each atom has core electron with the characteristic binding energy. The energy of the X-ray photon is adsorbed completely by the core electron of an atom when an X-ray beam hits the sample. The core electron will escape from the atom and emit out of the surface, if the

incident photon energy, hν is large. The emitted electron with the kinetic energy E_k is referred to as the photoelectron. The Einstein relationship gives the binding energy of the core electron is as follows:

$$h\nu = E_b + E_k + \phi$$

$$E_b = h\nu - E_k - \phi$$

Where hν (1486.6 eV) is the X-ray photon energy; E_k is the kinetic energy of photoelectron, which can be measured by the energy analyzer and ϕ is the work function of the analyzer which is about 4-5 eV.

Experimental set-up:

The experimental set-up consists of three main components:

(i) A photon source

(ii) Energy analyzer for photoelectrons

(iii) An electron detector

A high vacuum is required to increase the mean free path of the electrons coming out of the sample surface and to reach the detector, and to remove the contamination over the sample surface during measurement.

Charge correction

Sample charging is an important phenomenon in XPS. The sample surface gets positively charge due to continuous release of photoelectrons. The KE reduces as the positively charged surface attracts the outgoing photoelectron which resulted to the shift in

photoelectron peaks towards higher binding energy. In order to overcome the sample charging, surface of the sample is grounded by applying silver paste. It provides a conducting path between sample surface and metallic holder which is grounded. Depending on the nature of the samples sometimes the charging may still take place.

In the present study, we have employed XPS instrument of AMICUS using Al-K_α radiation. The vacuum level of the sample preparation chamber (SPC) was ~10^{-8} Torr and the sample analysis chamber (SAC) was ~10^{-9} Torr. The sample was scanned over the full energy range (survey scan) and then specifically selected 1s, core level spectra of Co 2p, Zn 2p, Cr 2p are scanned for present study. As carbon is usually present on the sample surface as contamination layer, the carbon C1s peak was recorded in the data. Charging of the sample shifts the C1s peaks and also sample's XPS peaks towards higher binding energy by same amount. The amount of charging can be measured by calculating the shift of C1s peak from the reference value, i.e. 284.6 eV. The charge correction is done by subtracting the difference value from the raw XPS data. XPS data were fitted using XPSPEAK 4.2 software package. The background was set as linear and peaks are added in the appropriate position. All parameters like peak position, full width half maximum (FWHM), area and percentage of Lorentzian and/or Gaussian distribution was optimized. Finally, all peaks including satellite peaks were optimized and fitted.

3.2.3 Extended X-ray Absorption Fine Structure (EXAFS)

X-ray absorption spectroscopy is a sophisticated technique to study the structural characterization of local atomic environment of the element of interest. The bond distances, coordination numbers and type of nearest neighbors surrounding the central

atom can be investigated using X-ray absorption spectroscopy. X-ray absorption refers to the details of how X-rays absorbed by an atom at energies near and above the core-level binding energies of that particular atom. The most intense source of monochromatic beam of X-rays from synchrotron is directed through a homogeneous sample. According to Lambert-Beer law, the attenuation of energy of the X-rays (E) can be described by $I(E) = I_o(E)e^{-\mu(E)x}$

Where, $I_o(E)$ and I(E) are the incident and transmitted X-ray intensities, and $\mu(E)$ is the linear absorption coefficient (or attenuation coefficient) which describes how strongly X-rays are absorbed as a function of X-ray energy. It depends on both absorption of x-rays and the Bragg scattering of x-rays out of the incident beam.

X-ray absorption spectroscopy is a measure of transitions from core electronic states of the material to the excited electronic states and the continuum; the former is known as X-ray absorption near-edge structure (XANES), and the latter as extended X-ray absorption fine structure (EXAFS). EXAFS studies the absorption at energies greater than the threshold for electron release. XANES energy ranges up to ~ 60 eV above the edge while EXAFS ranges from 60 eV to 1200 eV above the edge. The XANES spectra data provides information about electronic structure and symmetry of the metal site and EXAFS spectroscopy provides distances to ligands, nearest neighbor atoms from the absorbing element.

In, EXAFS, the energy of X-ray greater than the lowest unoccupied molecular orbital (LUMO) level provides sufficient energy to cause the absorbing atom to release the electron. The kinetic energy of the photoelectron is given by the following relation

$E-E_o=½\ m_e v^2$

Where E is the X-ray photon energy, E_o is the ionization or threshold energy for the electron, and m_e is mass of the electron. The EXAFS modulations are better expressed as a function of the photoelectron wave vector k ($k=2\pi/\lambda$). Using the de Broglie relation, $\lambda= h/ m_e v$, h is a plank's constant, the above expression is changed as

$$k = \frac{2\pi}{h}[2\ m_e(E - E_0)]^{1/2} = 0.512\ (E - E_0)^{1/2}$$

where, E and E_0 are expressed in electron volts (eV) and the units of k is ($Å^{-1}$).

The departing electron wave interfere owing to the scattering off nearby atoms. The resulting interference is between the outgoing photoelectron wave and components of backscattered wave from neighboring atoms in the molecule. In EXAFS, the oscillatory portion of the absorption coefficient, the difference between the observed absorption coefficient $\mu\ (k)$ and the free-atom absorption coefficient, k, normalized by the free-atom contribution:

$$\chi(k) = \frac{\mu(k)-\mu_o(k)}{\mu_O(k)}$$

In order to visualize the information of an EXAFS spectrum, Fourier transformation has been used. The Fourier transformation of $\chi(k)$ is defined as

$$FT(R) = \frac{1}{\sqrt{2\pi}}\int_{k_{min}}^{k_{max}} K^n\ \chi(k)\ e^{i2kR}\ dK$$

A pseudo-radial distribution function is obtained from the the canonical variables k ($Å^{-1}$) and R (Å) and Fourier transform of an EXAFS spectrum. The FT is used for qualitative analysis of shells in a system.

Experimental setup

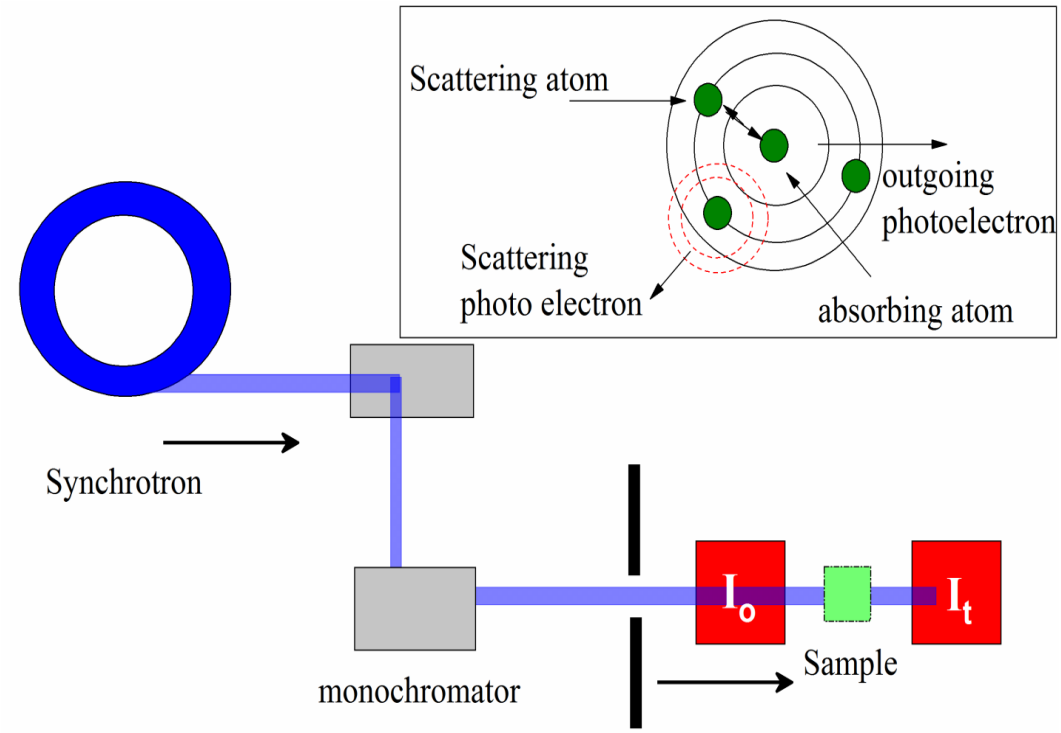

Fig. 3.2.3 The experimental set-up of EXAFS; Inset shows the scattering of photoelectron after incident atomic absorption.

Data analysis

In order to determine the average coordination structure around the absorber atom, a theoretical model for the sample is designed with which EXAFS data could be generated using computer program like FEFF (which stands for f_{eff}, the effective scattering amplitude). The software program Artemis is available for computing theoretical EXAFS models. Using Artemis software, one can adjust the structural parameters in the EXAFS

equation until least-squares fit is obtained between the theoretical and the experimental spectra. In order to isolate the contribution of the short scattering paths, EXAFS data is fitted in R space using Fourier transform. The parameters that are determined from the fitting of the theoretical model with the experimental EXAFS data are N (coordination number), S_o^2, σ^2, ΔE_o and ΔR. While the parameters N, S_o^2 and σ^2 affect the amplitude of the EXAFS oscillations and the phase of the oscillation is affected by ΔE_o and ΔR (Kelly *et al.*, 2008).

In the present study, EXAFS measurements were carried out at the energy scanning EXAFS beam line (BL-9) in transmission mode at INDUS-2, synchrotron source (2.5 GeV, 100 mA) at the Raja Ramanna Centre for Advanced Technology (RRCAT), Indore, India. Samples of an appropriate weight was mixed thoroughly with cellulose powder to obtain a total weight of 100 mg. Hydraulic press was used to prepare pellets of 15 mm diameter. EXAFS data analysis programs available within the IFEFFIT software package were used for analysis. ATHENA software was used for EXAFS data processing including conversion of raw data to $\mu(E)$ spectra, background subtraction, Fourier transformation and for plotting. ARTEMIS software was used to fit the experimental data with the theoretical spectra. It is well known that σ^2, the amplitude function, which is the mean-square displacement of the path-length due to the thermal or static disorder and is strongly correlated with the number of nearest neighbors. Lattice parameters and atomic coordinates are used as inputs to generate a FEFF input file.

3.2.4 Scanning electron microscope (SEM)

Scanning electron microscope is an advanced model of an electron microscope which is used to study the three dimensional image of the specimen.

Principle

The secondary electrons generated when highly accelerated primary electrons are focused on the sample. These secondary electrons create a three dimensional image of the sample. It is used to study the topography, morphology like shape and composition of particles. The relative amount of elemental composition of a material and crystallographic information like arrangement of atoms in the material is visualized.

Construction and working

It consists of an electron gun, magnetic condensing lens, scintillation detector and a video amplifier. The electron gun produces a highly energetic beam of electrons. A magnetic condensing lens is used to focus the electron beam which is followed by a scanning coil. The electron detector is used to collect the secondary electrons scattered from the sample and converts them into electric signals. These signals are passed through cathode ray oscilloscope (CRO) through video amplifier. An Energy Dispersive X-ray Spectroscopy (EDS) detector consists of a crystal that absorbs the energy of the incoming X-rays by ionization. This yields free electrons in the crystal which becomes conductive and produces an electrical charge. The X-ray absorption thus converts the energy of individual x-rays into electrical voltages of relative size.

For the present study, field emission gun based scanning electron microscope (FE-SEM) of SUPRA 40, ZEISS, made in Germany was used. $CoCr_2O_4$ and Zn doped $CoCr_2O_4$ samples were mounted on the sample holder using carbon tape. The voltage of electron gun was applied upto 30 kV to capture well focused image. Compositional analysis was carried out by the energy dispersive x-ray spectroscopy (EDS) available with the above system.

3.2.5 Transmission electron microscope (TEM)

The transmission Electron Microscope (TEM) is a powerful technique for probing the structure of materials. TEM is used to characterize the morphological information like shape, size and distribution of nanoparticles. TEM is available in several different forms like HRTEM (High resolution TEM), STEM (Scanning TEM) and ATEM (Analytical TEM).

Experimental setup

TEM comprises of an electron gun, a vacuum system, electromagnetic lenses, high voltage generator, recording devices and the associated electronics. The resolution of the modern TEM is under 0.2 nm even with a fair amount of specimen tilt. TEM uses electrons of lower wavelength which makes it possible to get a high resolution image. A well focused electron beam obtained from electron gun assembly and electromagnetic condenser lenses is accelerated by an anode, which is typically at +100 KeV with respect to the cathode. The beam is restricted by the condenser aperture, which stops un-collimated electrons. The collimated high energy (200 KeV and above) beam of electrons strikes the specimen and gets scattered depending upon the thickness and specimen

electron transparency. Part of the scattered electron beam undergoing phase and amplitude change during scattering is transmitted and the same is focused by the objective lens which forms an image on phosphor screen or charge coupled device camera. To block the high-angle diffracted electrons, objective apertures can be adjusted in order to enhance the contrast.

There are two basic modes of TEM operation: diffraction patterns and imaging modes. Modern TEM has about five to six image forming lenses. If the lenses are excited in such a way that these back image plane of the objective lens as an object then what we see on the screen is the image of specimen. In modern TEM, it is possible to switch from diffraction to imaging and vice-versa by changing the excitation of the lenses following the objective lens.

Data analysis

The well distributed particles of TEM image could be analyzed for shape and size distribution. The histogram of particles distribution (particles size vs. number of particles) is plotted with the help of Image J software. Fitting of the data using Lorantzian distribution provides the average particle size. The selective area electron diffraction (SAED) pattern shows well concentric rings of different radii. The diffraction rings are indexed by calculating inverse of its radii and matching it with inter-planar spacing (d) in reciprocal space of XRD data using WinPLOTR software.

High Resolution Transmission Electron Microscopy (HRTEM)

High-resolution TEM is an imaging mode of the TEM that provides the imaging of the crystallographic structure of a sample at atomic scale. The transmitted and

scattered beams are used to create an interference image. The phase contrast image of HRTEM can be as small as the unit cell of a crystal. It can produce images with high resolution below 0.1 Å at magnification above 50 million times. The basic alignment of TEM and sample were height, orientation, rotation center, defocus, astigmatism etc. The voltage applied for the electron gun is 200 kV. The well distinguished atomic planes of HRTEM were indexed by calculating the interplanar distance and were compared with the XRD data to confirm the phase.

3.2.6 Magnetic measurements

Magnetic properties of the materials are studied by measuring temperature and field dependent magnetizations using vibrating sample magnetometer (VSM). In this work, we have used Physical Property Measurement System (PPMS), Magnetic Property Measurement System (MPMS) of Quantum Design, USA. The frequency dependence of magnetization is studied using Superconducting Quantum Interference Device (SQUID) magnetometer.

The description of VSM and SQUID magnetometer are given below.

3.2.6.1 Vibrating Sample Magnetometer (VSM)

Vibrating sample magnetometer is used to measure the magnetic moment of the sample with very high precision. The sample undergoes a vertical motion with a frequency 60-80 Hz and amplitude 1 mm. The sample rod is kept in between two pick-up coils under the highly homogeneous magnetic field. The vibrating component causes a change in the magnetic field around the sample. The change in the magnetic flux induces

a voltage in the sensing coil (pick-up coil). According to Faraday's law, the voltage in a single winding of the pick-up coil can be written as

$$U_{ind} = - \frac{d\varphi}{dt}$$

U_{ind} and φ are induced voltage and magnetic flux respectively. The rate of change of magnetic flux is proportional to the voltage developed in the pick-up coils and is directly related to the magnetic moment of the sample. The moment observed here is irrespective of the strength of applied field.

Fig. 3.2.4 MPMS-3, Quantum Design (USA) used for magnetic measurement.

The VSM (MPMS) used in the present work have a multiple measurement modes with a range of temperatures from 1.8 K to 400 K and magnetic field ranges from ±

0.05 Oe to maximum ± 70 kOe. The PPMS used for the present work having specification with temperature ranging from 2 to 400 K and field used up to 140 kOe.

3.2.6.2 SQUID magnetometer

SQUID magnetometer is one of the most sensitive and effective device to measure the magnetic properties of materials. This is a direct method to measure the magnetic moment of a sample in absolute units. The device configured with a magnetometer to detect small magnetic fields. SQUID consists of two superconductors separated by thin insulating layers to form two parallel Josephson junctions. In Josephson junction, the electrical current density through a weak electric contact between two superconductors depends on the phase difference Δφ of the two superconducting wave functions. The time derivative of Δφ is correlated with the voltage across the weak contact. Hence, the setup of superconducting ring with two Josephson junctions could be used to convert magnetic flux in to an electric voltage.

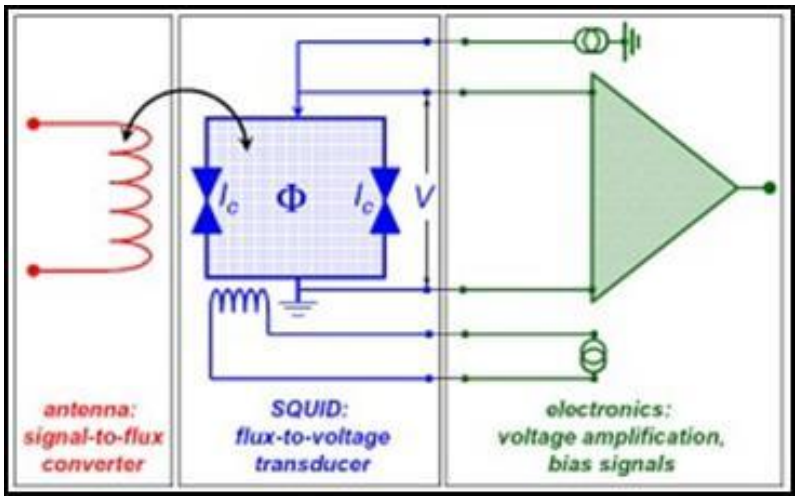

Fig. 3.2.5 Schematic diagram of SQUID magnetometer.

SQUID magnetometer consists of 3 main parts: The SQUID which is a main unit (blue), magnetic flux transformer (red) and the electronics for voltage amplification. A magnetic shielding is provided to the sensor to avoid the fluctuations from the ambient magnetic field of the laboratory and from the magnetic field produced by the superconducting coil. The SQUID magnetometer used in the present work is MPMS EverCool system with an integrated cryocooler dewar system. It has a highest sensitivity of $5x10^{-8}$ emu and frequency range of 0.1 Hz - 1 KHz. In this system, direct phase nulling technique measures and cancels background AC phase shifts at every measurement. The rate of temperature change was 10 K/min from 300 K to 10 K and was 2 K/min from 10 K to 2 K. The frequencies used for the ac susceptibility measurement are 3, 31, 230 and 966 Hz. In all samples real and imaginary parts of susceptibility were measured with varying temperature and keeping frequency constant.

3.2.7 Diffused Neutron Scattering (DNS)

Diffused neutron scattering is a versatile technique in which cold neutrons undergo diffuse scattering in time-of-flight spectrometer with polarization analysis. The neutron time-of-flight diffraction is an appropriate technique as the diffused scattering of neutrons occurs throughout the reciprocal space. Using this technique, large volumes of reciprocal space can be accessed in a single measurement. In general, unpolarized neutrons are used to investigate the periodicity and magnitude of the magnetic order while spin-polarized neutrons could be used to reveal the direction of the atomic magnetic moments. DNS with a polarization analysis is complementary to standard neutron powder diffraction. It is mostly used for magnetic structure

refinements of samples having small moments by amplifying the signal to noise ratio. Diffused scattering gives information on the short range order in a material.

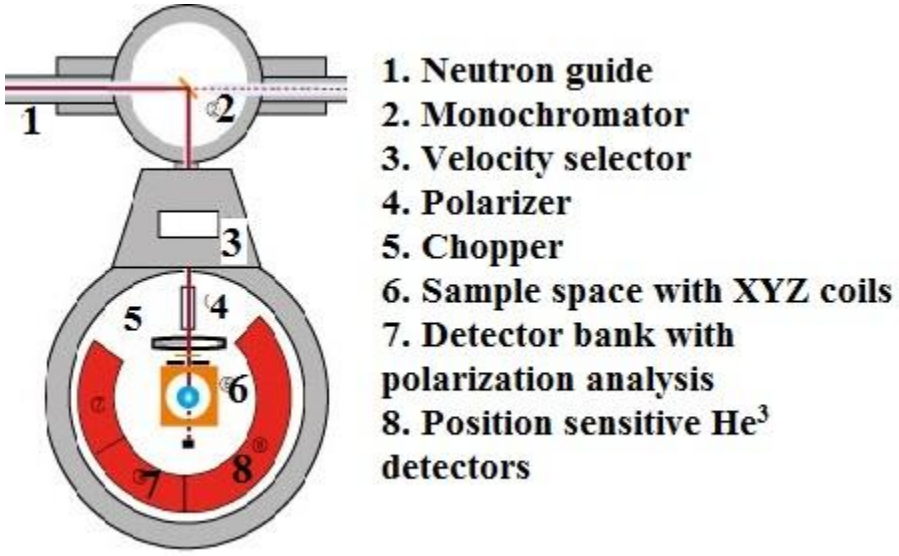

Fig. 3.2.6 The block diagram shows different parts in diffused neutron scattering experiment [From http://www.nffa.eu].

The experimental block diagram of DNS is shown in Fig. 3.2.6. The incident neutrons from a single crystal monochromator are purged of λ/2 contamination with a Be-filter, polarized with a super mirror bender and passes through a flipper. The monochromator is horizontally and vertically adjustable and double focusing. The wavelength range of monochromator is 2.4 Å ≤ λ≤ 6 Å. The chopper frequency is less than or equal to 300 Hz. The sample is mounted inside the cryostat and can be turned to an angle Θ. The monoenergetic neutron pulse collides with the sample and exchanges their energy during scattering. The scattered neutrons are detected within an angle 2Θ by multiple detector bank where each detector is placed behind a bender polarization analyzer. The 25 detectors set are placed at 85 cm distance to the sample, covers a wide

angle of 125^{o}. The final energy of the neutron is determined from the arrival time at the detectors. XYZ-polarization analysis allows the separation of nuclear coherent, spin incoherent and magnetic scattering contributions simultaneously over a large range of scattering vector, Q and energy transfer, E. The neutron magnetic moment makes neutrons scatter from magnetic structures or magnetic field gradients.

Fig.3.2.7 DNS experimental setup at FRM II, JCNS, Forschungszentrum Julich GmbH, outstation at the Heinz Mailer-Leibniz Zentrum (MLZ), Germany. [From https://physicsworld.com]

In the present study, we carried out polarized neutron scattering measurement using Diffused Neutron Scattering (DNS) spectrometer with polarization, at FRM II, which is operated by Jülich Centre for Neutron Science (JCNS), Forschungszentrum Julich GmbH, outstation at the Heinz Mailer-Leibniz Zentrum (MLZ), Garching, Germany. The sample environment is a top loading CCR and cold-cycle cold head. The

powder sample is taken in a cylindrical aluminum holder. A large double-focusing monochromator and a highly efficient supermirror-based polarizer provide a polarized neutron flux of about 10^7 n cm^{-2} s^{-1}. The wavelength of monochromator is 4.2 Å. The monochromator is horizontally and vertically adjustable one having double focusing. The raw data obtained from DNS consists of nuclear coherent, paramagnetic and spin-incoherent scattering in both spin flip and non spin flip states. The non-spin-flip scattering is sensitive only to those components of the magnetization parallel to the neutron spin. In contrast, the spin-flip scattering is sensitive only to those components of the magnetization perpendicular to the neutron spin. The incoherent pattern should be flat and the magnetic neutron scattering can be associated with a spin flip of the neutron. Plot.py software was used to process the raw diffused neutron scattering data. The magnetic scattering should be separated from the nuclear-coherent and spin-incoherent contributions using XYZ-polarization analysis. Approximately 2.5 g of sample was kept in an aluminium sample holder of radius 12 mm for the measurement. The measurement temperature range varied from 3.5 K to 100 K for all sample. The six polarized scattering contributions by sample as well as Ni0.89Cr0.11 standard and vanadium references were measured in a wide scattering momentum range of $0.5<Q<3.4$ $Å^{-1}$.The measurements were carried out using aluminium sample holder in a temperature range of 3.5 K to 100 K. The magnetic, nuclear and nuclear spin-incoherent scattering contributions were separated from the total scattering cross section by means of XYZ-polarization analysis in the spin flip (SF) and non-spin flip (NSF) channels. Using DNS polarization analysis algorithm, the data was separated. The reference measurement of a $Ni_{0.89}Cr_{0.11}$ alloy yields the flipping ratio correction and thus the real polarization of the

incident neutron beam. Background correction is performed by measurement of the empty aluminium sample holder. Detector efficiency was obtained by calibration of empty vanadium holder. The background data measured for an empty sample holder was subtracted and the detector sensitivity was corrected using a measurement from an incoherent scatterer to scale the intensities of each detector.